Mach cone signal and energy deposition scenarios in linearized hydrodynamics

R. B. Neufeld[1,*] and Thorsten Renk[2,3]

[1]*Los Alamos National Laboratory, Theoretical Division, MS B238, Los Alamos, New Mexico 87545, USA*
[2]*Department of Physics, P.O. Box 35, University of Jyväskylä, Jyväskylä FI-00014, Finland*
[3]*Helsinki Institute of Physics, P.O. Box 64, University of Helsinki, Helsinki FI-00014, Finland*

Particle correlation measurements associated with a hard or semihard trigger in heavy-ion collisions may reflect Mach cone shock waves excited in the bulk medium by partonic energy loss. This is of great interest because, when compared with theory, such measurements can provide information on the transport properties of the medium. Specifically, the formation of Mach cone shock waves is sensitive to the viscosity and speed of sound, as well as the detailed nature of the jet-medium interaction. However, modeling the physics of shock-wave excitation to obtain a meaningful comparison with measured correlations is very challenging, as the correlations arise from an interplay of perturbative as well as nonperturbative phenomena at different momentum scales. In this work we take a step in that direction by presenting a systematic study of the dependence of azimuthal particle correlations on the spatiotemporal structure of energy deposition into the medium. Our results indicate that detailed modeling of the evolution of an initially produced hard parton and the interaction of this evolving state with the medium is crucial, as both the magnitude and the shape of the shock-wave signal show a strong dependence on the assumptions being made.

I. INTRODUCTION

It is useful to describe the dynamics in ultrarelativistic heavy-ion collisions in terms of the "bulk" and of "probes." The bulk medium, that is, the quark-gluon plasma (QGP), describes QCD matter produced in the collision that is strongly coupled, exhibits collectivity, and behaves like a thermalized, near-perfect liquid. The bulk matter is chiefly responsible for the properties of low-transverse-momentum (P_T) hadron production. In contrast, there are also hadrons produced at higher momenta that are clearly not thermalized. Such hadrons originate from hard partonic processes that probe such small time and distance scales that they are essentially unmodified by the medium. However, these high-p_T partons undergo a final-state interaction while they propagate through the medium before hadronization. This "jet quenching" [1–6] has been expected by theory and is experimentally confirmed in measurements of the nuclear suppression factor R_{AA} [7].

If there is energy loss from a high-p_T parton, energy conservation requires that this lost energy flows somewhere. Measurements of particles associated with a high-P_T trigger hadron [8,9] have given a hint to answering this question: Instead of a back-to-back jetlike correlation structure on the near (trigger) side and the away side as observed in d-Au collisions, the observed correlation shows a surprising splitting of the away-side peak into a double-hump structure. Early on, this was interpreted as the reaction of the bulk medium to the hard probe in terms of a shock wave [10], and early phenomenological investigations with a fluid-dynamics-inspired approach to propagate the shock wave in the background of an evolving bulk medium and with a full modeling of the trigger bias [11–13] have confirmed that a shock-wave

signature is not erased by medium-flow-induced distortion or by averaging over many different triggered events but can, indeed, account for the correlation observed in the data. Since then, the focus has been on a more rigorous theoretical formulation of coupling a source of energy and momentum into the hydrodynamical equations using hard thermal loop or anti-de Sitter space/conformal field theory methods [14–18].

In bringing such proof-of-concept calculations closer to a comparison with data, one of the key questions is the time dependence of the energy and momentum deposition into the medium. In this paper, we make the assumption that the energy and momentum absorbed by the medium are related by an on-shell condition so that $\mathbf{u}dE/dt = d\mathbf{p}/dt$ (see Sec. II C), where dE/dt and $d\mathbf{p}/dt$ are the energy and momentum deposition rates, respectively, and $\mathbf{u}$ is the velocity of the high-p_T parton. For this reason, we focus on the time dependence of the energy deposition, which is potentially driven by many different effects. First, the strength of the interaction between hard parton and medium depends on the medium density, and in a real heavy-ion collision this density varies as a function of space roughly as given by the nuclear overlap and, owing to the expansion of the medium, also drops as a function of time. The expansion dynamics therefore tends to lead to less interaction with the medium and hence less energy loss at late times. In contrast, radiative energy loss in a constant medium of length L has a characteristic L^2 dependence owing to Landau-Pomeranchuk-Migdal suppression of near-collinear gluon radiation, and this effect tends to increase energy loss at late times, to some degree even in an expanding medium. In addition, in Ref. [19] it was suggested that gluons radiated from a hard parton subsequently themselves interact with the medium and hence contribute to the energy flow into the medium, leading to a "crescendo" in the shock-wave excitation and a large energy deposition at late times. In contrast, low-energy partons undergoing strong energy loss

cannot act for a long time as sources of energy, but become absorbed by the medium after just a short time. This effect again tends to lead to small energy deposition at late times, as energy deposited into the medium early on is not available later.

The arguments given so far assume that the source of energy and momentum entering the medium is a single on-shell parton that subsequently undergoes interactions leading to induced gluon radiation. However, in a typical hard event, partons are produced with large initial virtualities and, even in vacuum, evolve into a parton shower where the individual quanta have lower virtualities, and the time scale of the shower evolution is such that it takes place at least partially before a medium is produced. This implies that it may be wrong to think of a single parton initially depositing energy into the medium: The dynamics may rather be that a developed parton shower acts as a strong source initially, but energy deposition decreases rapidly, as the energy of subleading shower partons is quickly depleted.

It follows from the preceding that modeling the time dependence of energy deposition correctly is not a simple and straightforward issue. It is the purpose of this paper to demonstrate that the question is nevertheless highly relevant: Modeling the time dependence of energy deposition in a different way alters both the magnitude and the shape of the shock-wave signal in a significant way. We illustrate this point by using different model assumptions for the energy deposition within a constant medium and solving linearized hydrodynamical equations. The paper is organized as follows: In Sec. II A we review the underlying formalism of linearized hydrodynamics, while in Sec. II B we discuss how to obtain the azimuthal hadron spectrum from the linearized equations of motion. In Sec. II C we discuss the motivation for the form of the hydrodynamic source term used in our results and show how it depends sensitively on the time dependence of the energy deposition. In Sec. II D we present the different energy deposition scenarios used in our results and discuss the underlying physics assumptions of each one. The reader interested only in the results of our calculations can skip directly to Secs. III A and III B, where specific numerical inputs and resulting azimuthal spectrums are presented.

II. MEDIUM EXCITATION

A. Linearized hydrodynamics

In what follows we consider a hard parton (parton here refers to the parent parton and the associated secondaries) propagating in an infinite and static QGP. Additionally, we ignore any net baryon density, which is a reasonable assumption for relativistic heavy-ion collision energies at midrapidity [21]. This parton acts as a source of energy and momentum that is coupled to the linearized hydrodynamic equations of the underlying medium. The linearized approximation is valid when the energy and momentum density generated by the hard parton is low compared to the equilibrium energy density of the medium. More is said on the linearized approximation in Sec. III.

The assumption of an infinite and static QGP is clearly unrealistic for heavy-ion collisions. However, our purpose here is not to present a study that is directly comparable to experimental data but, rather, to show the effect of the time dependence of energy deposition on the azimuthal particle spectrum associated with a hard parton. The linearized approximation in a static medium is a good toy model for such a study because the effect of changing parameters such as viscosity or energy deposition scenarios can be easily extracted. Even within the linearized approximation one could go beyond the static medium, for instance, by assuming an underlying Bjorken expansion. This would introduce complications associated with underlying flow fields and boundary conditions, however, and is beyond the scope of the current paper.

In the linearized approximation, the effect of the source is to create a local perturbation in the medium, so that the energy-momentum tensor has the linearized form

$$T^{\mu\nu} = T_0^{\mu\nu} + \delta T^{\mu\nu}, \tag{1}$$

where $\delta T^{\mu\nu}$ is the perturbation generated by the source, and $T_0^{\mu\nu}$ is the equilibrium energy-momentum tensor of the underlying medium. The fast parton's ability to perturb the medium is encoded in the source term, J^ν (specified later), which couples to the gradient of the energy-momentum tensor

$$\partial_\mu \delta T^{\mu\nu} = J^\nu, \tag{2}$$

where $\partial_\mu T_0^{\mu\nu} = 0$.

The equations of motion for a medium coupled to a source in linearized hydrodynamics are discussed in several places (e.g., Refs. [10] and [16]). The solution for $\delta T^{\mu\nu}$ in terms of J^ν is most easily expressed in momentum space by taking the Fourier transform of (2). The result to first order in shear viscosity η for the perturbed energy density $\delta T^{00} \equiv \delta\epsilon$ and momentum density $\delta T^{0i} \equiv \mathbf{g}$ are given by

$$\delta\epsilon(\mathbf{k}, \omega) = \frac{ik J_L(\mathbf{k}, \omega) + J^0(\mathbf{k}, \omega)(i\omega - \Gamma_s k^2)}{\omega^2 - c_s^2 k^2 + i\Gamma_s \omega k^2}, \tag{3}$$

$$\mathbf{g}_L(\mathbf{k}, \omega) = \hat{\mathbf{k}} g_L = \frac{i\omega \hat{\mathbf{k}} J_L(\mathbf{k}, \omega) + ic_s^2 \mathbf{k} J^0(\mathbf{k}, \omega)}{\omega^2 - c_s^2 k^2 + i\Gamma_s \omega k^2}, \tag{4}$$

$$\mathbf{g}_T(\mathbf{k}, \omega) = \mathbf{g} - \mathbf{g}_L = \frac{i\mathbf{J}_T(\mathbf{k}, \omega)}{\omega + \frac{3}{4}i\Gamma_s k^2}. \tag{5}$$

In the preceding result, c_s denotes the speed of sound, $\Gamma_s \equiv \frac{4\eta}{3(\epsilon_0 + p_0)} = \frac{4\eta}{3sT}$ is the sound attenuation length, ϵ_0 and p_0 are the unperturbed energy density and pressure, respectively, and s is the entropy density. Also, the source and perturbed momentum density vectors are divided into transverse and longitudinal parts: $\mathbf{g} = \hat{\mathbf{k}} g_L + \mathbf{g}_T$ and $\mathbf{J} = \hat{\mathbf{k}} J_L + \mathbf{J}_T$, with $\hat{\mathbf{k}}$ denoting the unit vector in the direction of $\mathbf{k}$. The position space result for Eqs. (3)–(5) are obtained by reverse Fourier transform using the general rule

$$F(\mathbf{x}, t) = \frac{1}{(2\pi)^4} \int d^3k \int d\omega \, e^{i\mathbf{k}\cdot\mathbf{x} - i\omega t} F(\mathbf{k}, \omega). \tag{6}$$

B. The azimuthal spectrum

Once the source term has been specified, and a solution for $\delta\epsilon$ and $\mathbf{g}$ is obtained from Eqs. (3)–(6), we will be interested in determining the azimuthal particle spectrum generated by the source. Ignoring viscous corrections, the induced medium flow velocity is given by

$$\delta\mathbf{u}(x) = \frac{\mathbf{g}}{\epsilon_0 + p_0} = \frac{\mathbf{g}}{\epsilon_0\left(1 + c_s^2\right)}, \tag{7}$$

where we have used $c_s^2 = \partial p/\partial\epsilon \approx p_0/\epsilon_0$ for $T \gg T_c$ [22]. The total medium four-velocity, which is a sum of the underlying medium and induced velocities, is given by

$$[u_0 + \delta u(x)]^\mu = \left(1, \frac{\mathbf{g}}{\epsilon_0\left(1 + c_s^2\right)}\right), \tag{8}$$

where $\delta u^0 = 0$ in the limit of a static background. An expression for δT can similarly be found from dimensional considerations. We write the medium energy density as $\epsilon = AT^4$, where A is some constant, from which one has

$$\epsilon_0 + \delta\epsilon \approx AT_0^4\left(1 + 4\frac{\delta T}{T_0}\right), \tag{9}$$

leading to

$$\delta T(x) = \frac{\delta\epsilon}{4\epsilon_0}T_0. \tag{10}$$

Having expressions for the flow velocity and temperature, it is now possible to construct the medium's distribution function, which in the Boltzmann limit is given by

$$f(x, p) = e^{-\beta u^\mu p_\mu} = \exp\left[-\frac{[u_0 + \delta u(x)]^\mu p_\mu}{T_0 + \delta T(x)}\right]. \tag{11}$$

Here, $\beta \equiv 1/T$ is the inverse temperature. The distribution is converted into an azimuthal particle distribution by using a Cooper-Frye freeze-out scenario [23]. Consistent with the approach discussed in Refs. [17] and [18], the final azimuthal particle spectrum for massless particles at midrapidity ($y = 0$) is given by

$$\frac{dN}{dyd\phi}(y = 0) = \int_{p_T^i}^{p_T^f}\frac{dp_T\,p_T}{(2\pi)^3}\int d\Sigma_\mu p^\mu[f(x, p) - f_0], \tag{12}$$

where Σ_μ is the freeze-out hypersurface and

$$p^\mu = [p_T, 0, p_T\sin(\phi), p_T\cos(\phi)]. \tag{13}$$

The isotropic background contribution, $f_0 = e^{-\beta_0 u_0^\mu p_\mu}$, is subtracted in Eq. (12). In what follows, it is understood that the source parton propagates along the $\hat{z}$ axis, which also determines the direction of $\phi = 0$ in Eq. (13). We consider an isochronous freeze-out, as appropriate for a constant medium, in which case $d\Sigma_\mu = dV(1, 0)$.

C. The source term

Nothing has been said up to this point about the form of J^ν to be used in Eqs. (3)–(5). A common choice is the simple form

$$J^\nu(x) = \frac{dE}{dt}\delta(\mathbf{x} - \mathbf{u}t)U^\nu, \tag{14}$$

where $U^\nu \equiv (1, \mathbf{u})$, $\mathbf{u}$ is the velocity of the source parton, which is assumed to be at the origin at $t = 0$, and dE/dt is the time-dependent rate of energy loss into the medium (in principle, this can be less than the total rate of energy loss, if energy lost from a leading parton is, e.g., redistributed to nonthermalized degrees of freedom). This expression contains an eikonal assumption, as it describes a point source propagating with the speed of light on a straight line. The advantage of the source term in Eq. (14) is that it trivially conserves energy and momentum at each step in time. One can see this by integrating both sides of Eq. (2) over all space, from which it is found, for the $\nu = 0$ component, that

$$\frac{d}{dt}\int d\mathbf{x}\,\delta\epsilon = \frac{dE}{dt}, \tag{15}$$

which shows that the energy going into the medium is properly accounted for. A similar exercise holds for the other components of ν as well.

However, one can go beyond the simple form of Eq. (14) and still conserve energy and momentum at each step in time. Consider adding a total derivative to Eq. (14),

$$J^\nu(x) = \frac{dE}{dt}U^\nu\delta(\mathbf{x} - \mathbf{u}t) \rightarrow \frac{dE}{dt}(U^\nu - \lambda\partial^\nu)\delta(\mathbf{x} - \mathbf{u}t), \tag{16}$$

where λ is a coefficient with dimension of length. Again, integrating both sides of Eq. (2) over all space shows that energy and momentum are still properly accounted for. λ acts as a local medium excitation parameter; that is, its contribution integrates to 0 globally. The replacement in Eq. (16) is motivated by the form of the kinetic-theory-derived source term for a parton in a perturbative QGP obtained in Ref. [15] and is similar to the source term derived for a quark in a strongly coupled supersymmetric Yang-Mills plasma [25]. The relativistic limit ($\gamma \gg 1$) of the source derived in Ref. [15] can be put in the form

$$J^\nu = \frac{\alpha_s C_2 m_{\rm D}^2}{8\pi}\left((1, \mathbf{u})\frac{\gamma}{(\rho^2 + \gamma^2 z_-^2)^{3/2}} - \partial^\nu\frac{1}{2(\rho^2 + \gamma^2 z_-^2)}\right), \tag{17}$$

where C_2 is the Casimir of the source parton, m_D is the Debye screening mass in the medium, $\rho = \sqrt{x^2 + y^2}$ and $z_- = z - ut$ for a source parton propagating in the positive $\hat{z}$ direction, and $\gamma = 1/\sqrt{1 - u^2}$.

If one considers the source to be localized, Eq. (17) can be put into the mold of Eq. (16) by integrating the distributions over all space and normalizing to a δ function. It is helpful to add a damping factor, $e^{-\rho m_{\rm D}}$, to the distributions in Eq. (17), which regulates an infrared divergence that arises when integrating over all space. The form of our damping factor is motivated by the fact that medium-induced screening of the hard parton's color fields occurs on the Debye scale. The damping factor simulates the Debye screening of a Lorentz-contracted distribution, hence the form $e^{-\rho m_{\rm D}}$.

We find

$$\frac{e^{-\rho m_{\rm D}}\gamma}{(\rho^2 + \gamma^2 z_-^2)^{3/2}} \approx 4\pi G_0 \left(\frac{m_{\rm D}}{2\sqrt{E_p T}}\right)\delta(\mathbf{x} - \mathbf{u}t), \quad (18)$$

where $(2\sqrt{E_p T})^{-1}$ has been introduced as a short distance cutoff (E_p is the energy of the hard parton and T the medium temperature), and G_0 is a representation of the incomplete γ function

$$G_0(z) = \int_z^{\infty} dt \frac{e^{-t}}{t}. \quad (19)$$

One can also show that

$$\frac{1}{2(\rho^2 + \gamma^2 z_-^2)} \approx \frac{\pi^2}{\gamma m_{\rm D}}\delta(\mathbf{x} - \mathbf{u}t). \quad (20)$$

With these approximations, Eq. (17) is thus written in the form of Eq. (16) as

$$J^\nu = \frac{dE}{dt}(U^\nu - \lambda\partial^\nu)\delta(\mathbf{x} - \mathbf{u}t), \quad (21)$$

where

$$\lambda = \frac{\pi}{4\gamma m_{\rm D} G_0\left(\frac{m_{\rm D}}{2\sqrt{E_p T}}\right)} \quad (22)$$

and

$$\frac{dE}{dt} = \frac{\alpha_s C_2 m_{\rm D}^2}{2} G_0\left(\frac{m_{\rm D}}{2\sqrt{E_p T}}\right). \quad (23)$$

Localizing the source term to a δ function, as done in Eq. (21), has the advantage of making the linearized hydrodynamics easier to solve, but also has a physics justification. Hydrodynamics is a long-distance theory that assumes local thermal equilibrium, whereas energy deposition occurs on short distance scales and is a highly dissipative process. There is a natural separation of distance scales between the energy deposition and the medium response as described by hydrodynamics [in perturbation theory these scales are $1/(gT)$ and $1/(g^4T)$, respectively, where $g \ll 1$]. Localizing the source term to a δ function is consistent with this separation of scales.

As shown in the following results, the coefficient λ is especially important for generating Mach-like signals in the final azimuthal particle spectrum. This can be traced back to Eqs. (3)–(5). Equation (5) is a diffusion equation and the quantity $\mathbf{g}_T$ is the diffusive momentum density generated by the fast parton. Physically, the diffusive momentum contribution is a wake that flows in the direction of the fast parton's propagation and is not a sound wave. Previous studies [17,24] have shown that the diffusive momentum tends to fill up any double-peak structure in the final spectrum. In contrast, Eqs. (3) and (4) describe damped sound waves propagating at speed c_s: it is clear that $\delta\epsilon$ and $\mathbf{g}_L$ are the energy and momentum density carried by sound generated by the fast parton and will be responsible for Mach-like signals in the azimuthal spectrum. When writing a source of the form of Eq. (16) in momentum space, we find

$$J^\nu(\mathbf{k}) = \int d^4x\, e^{-i\mathbf{k}\cdot\mathbf{x}+i\omega t}\frac{dE}{dt}(t)(U^\nu - \lambda\partial^\nu)\delta(\mathbf{x} - \mathbf{u}t)$$

$$= \int_0^T dt \frac{dE}{dt}(t)e^{-ik_z t + i\omega t}(U^\nu + i\lambda k^\nu), \quad (24)$$

where a time derivative on dE/dt as well as boundary terms has been ignored, and the source is assumed to propagate from time $t = 0$ to time $t = T$. We discuss why we have dropped the derivative and boundary terms at the end of the results (Sec. III B). Here we simply note that the derivative term is numerically insignificant for the energy deposition scenarios we consider and that the boundary terms are an artifact of stopping and starting the source at a specific moment in time and obscure the physics we are trying to explore. It is immediately clear from Eq. (24) that the term proportional to λ does not excite the diffusive momentum density, which is generated by the transverse part of the source, but only excites the sound modes. The contribution to the medium excitation coming from the term proportional to λ is important for generating Mach-like signals in the final azimuthal particle spectrum.

In what follows, we use Eq. (24) as our source term, treating λ as an adjustable parameter and determining the rate of energy deposition dE/dt from different theoretical models discussed in Sec. II D. Our purpose here is not to suggest that the form of λ given in Eq. (22) is necessarily the correct form for the QGP created in heavy-ion collisions but, rather, to motivate the general form of the source, Eq. (21). The ansatz thus provides a connection between the hard, perturbative QCD physics of jet quenching and the soft, nonperturbative QCD physics of medium response.

D. Energy deposition scenarios

In the following, we investigate three scenarios for energy deposition into the medium. In all three cases, we assume that the medium properties do not change as a function of space or time during the energy deposition. With this assumption, the spatiotemporal structure of the energy deposition dE/dt is independent of changes in medium properties and is a function of the assumed physics of the source only. In addition, to study the dependence of the shock-wave signal on the functional form of dE/dt, we adjust the medium properties for each scenario such that the *integrated* energy deposition $\Delta E_{\rm tot} = \int_0^\infty dt\, dE/dt$ is the same. In contrast, if one would do calculations in a given microscopical model for parton-medium interactions and fix the medium to be, for example, at a given T, $\Delta E_{\rm tot}$ would *not* necessarily be the same in different scenarios of energy deposition.

We adopt the procedure of normalizing to the same $\Delta E_{\rm tot}$ nevertheless because the relevant microscopical degrees of freedom in the medium and their interaction with a hard probe are not known. In a more realistic model, with a hydrodynamically expanding medium, constraints from data on high-P_T observables could be utilized instead by requiring each of the energy deposition scenarios to agree with the observed suppression of high-P_T hadrons. In the absence of such data for a constant model, requiring the same $\Delta E_{\rm tot}$ is a substitute for such a constraint.

In the first scenario, we assume that the source entering the medium is given by a single on-shell parton that interacts with the medium only elastically. The energy transfer into the medium is then given by the expression [26]

$$\left(\frac{dE}{dt}\right)_C = \frac{\alpha_s C_2 m_D^2}{2} \ln \frac{2\sqrt{E_p T}}{m_D}, \quad (25)$$

where $\alpha_s = g^2/(4\pi)$ is the strong coupling, $m_D = gT$ the Debye mass, C_2 the appropriate color factor for a quark (4/3) or a gluon (3), and E_p the energy of the hard parton. Under the assumption that the hard parton is sufficiently energetic such that $E_p \gg \Delta E_{\text{tot}}$, the weak dependence on E_p can be neglected and $(\frac{dE}{dt})_C$ assumes a constant value if the medium temperature remains unchanged. Given this functional shape of dE/dt, we henceforth refer to this scenario as Flat.

In the second scenario, we still assume that the source entering the medium is a single on-shell parton with sufficient energy such that $E_p \gg \Delta E_{\text{tot}}$ is realized, but we also allow for inelastic interactions of this parton with the medium that induce radiation. As outlined in Ref. [19] (see also Ref. [20]), the gluons radiated from the hard parent partons become themselves sources of elastic energy loss with the medium and can also be absorbed by the medium if their energy becomes $O(T)$.

In this formalism, the effect of radiated gluons depositing energy into the medium can be cast in the form of an evolution equation for the distribution function $f(\omega, t)$, which describes the distribution of radiated gluons in the medium at time t with energy ω. This evolution equation reads

$$\frac{\partial}{\partial t} f(\omega, t) - \frac{\partial}{\partial \omega}[\epsilon(\omega)f(\omega, t)] = \frac{dI}{d\omega dt}(\omega, t), \quad (26)$$

where $\epsilon(\omega)$ is the collisional energy loss rate for gluons obtained from Eq. (25) as

$$\epsilon(\omega) = \frac{3}{2}\alpha_s m_D^2 \ln \frac{2\sqrt{\omega T}}{m_D}, \quad (27)$$

and in the Armesto-Salgado-Wiedemann formalism [27] the spectrum of radiated gluons is given by

$$\frac{dI}{d\omega dt} = -\frac{\sqrt{\hat{q}}\alpha_s C_2}{\pi}\text{Re}\frac{(1+i)\tan\left[(1+i)\sqrt{\frac{\hat{q}}{\omega}\frac{t}{2}}\right]}{\omega^{3/2}}, \quad (28)$$

where

$$\hat{q} = 2\alpha_s C_2 m_D^2 T \ln \frac{2\sqrt{E_p T}}{m_D} \quad (29)$$

is used to adjust the strength of the inelastic interactions.

Equation (26) must be solved numerically. Given such a solution, the rate of energy gained by the medium from radiated gluons is [19]

$$\left(\frac{dE}{dt}\right)_R = \int_{\omega_{\text{min}}}^{\omega_{\text{max}}} d\omega \epsilon(\omega) f(\omega, t) + \int_0^{\omega_{\text{min}}} d\omega \omega \frac{dI}{d\omega dt}$$
$$+ \omega_{\text{min}} f(\omega_{\text{min}}, t)\epsilon(\omega_{\text{min}}) \quad (30)$$

where $\omega_{\text{min}} = T$ and $\omega_{\text{max}} = E_p/2$. The total energy deposition into the medium is then given as the sum of the collisional and radiative contributions,

$$\frac{dE}{dt} = \left(\frac{dE}{dt}\right)_C + \left(\frac{dE}{dt}\right)_R \quad (31)$$

where $(dE/dt)_C$ is obtained from Eq. (25). This second scenario leads to an increase in $\frac{dE}{dt}$ in time, therefore it has been named Crescendo.

In the third scenario, we take the source entering the medium to be a highly virtual parton that subsequently evolves into a parton shower. In addition, we do not make the assumption $E_p \gg \Delta E_{\text{tot}}$ but consider finite energy kinematics for all partons. For this, we utilize the Monte Carlo code YaJEM (yet another jet energy-loss model) [28,29]. In the following, we summarize the essential parts of the computation; details are given in Ref. [29]. (The scenario used in this paper corresponds to the DRAG (medium-induced drag force) scenario described in Ref. [29].)

We model the evolution from the initial parton to a final-state parton shower as a series of branching processes $a \rightarrow b + c$, where a is called the parent parton and b and c are referred to as daughters. In QCD, the allowed branching processes are $q \rightarrow qg, g \rightarrow gg$, and $g \rightarrow q\bar{q}$. The kinematics of a branching is described in terms of the virtuality scale Q^2 and of the energy fraction z, where the energy of daughter b is given by $E_b = zE_a$, and that of the daughter c by $E_c = (1-z)E_a$. It is convenient to introduce $t = \ln Q^2/\Lambda_{\text{QCD}}$ where Λ_{QCD} is the scale parameter of QCD. t takes a role similar to that of time in the evolution equations, as it describes the evolution from some high initial virtuality Q_0 (t_0) to a lower virtuality Q_m (t_m) at which the next branching occurs. In terms of the two variables, the differential probability dP_a for a parton a to branch is [30,31]

$$dP_a = \sum_{b,c} \frac{\alpha_s}{2\pi} P_{a \rightarrow bc}(z) dt dz, \quad (32)$$

where the splitting kernels $P_{a \rightarrow bc}(z)$ read

$$P_{q \rightarrow qg}(z) = 4/3 \frac{1+z^2}{1-z}, \quad (33)$$

$$P_{g \rightarrow gg}(z) = 3 \frac{[1-z(1-z)]^2}{z(1-z)}, \quad (34)$$

$$P_{g \rightarrow q\bar{q}}(z) = N_F/2[z^2 + (1-z)^2]. \quad (35)$$

We do not consider electromagnetic branchings. N_F counts the number of active quark flavors for given virtuality. The resulting system of equations describing the branching processes in vacuum is solved numerically using Monte Carlo techniques utilizing the PYSHOW code [32].

To make the link from momentum space, where the shower evolution takes place, to position space, where the medium perturbations evolve, we assume that the average formation

time of a shower parton with virtuality Q is developed on the time scale $1/Q$; that is, the average lifetime of a virtual parton with virtuality Q_b coming from a parent parton with virtuality Q_a is in the rest frame of the original hard collision (the local rest frame of the medium may be different by a flow boost, as the medium may not be static) given by

$$\langle \tau_b \rangle = \frac{E_b}{Q_b^2} - \frac{E_b}{Q_a^2}. \tag{36}$$

We assume that the actual formation time can then be obtained from a probability distribution,

$$P(\tau_b) = \exp\left[-\frac{\tau_b}{\langle \tau_b \rangle}\right], \tag{37}$$

which we sample to determine the actual formation time of the fluctuation in each branching.

We assume that the medium induces an approximately constant energy loss on each propagating parton. The medium is then characterized by a drag coefficient D that describes the energy loss per unit path length. In the simulation, the energy (and momentum) of each propagating parton is reduced by

$$\Delta E_a = \int_{\tau_a^0}^{\tau_a^0 + \tau_a} d\zeta \, D. \tag{38}$$

For a propagating gluon the energy loss is increased by the color factor ratio 2.25. While Eq. (38) describes the mean energy loss, the actual energy loss owing to the medium is randomized in each event.

The dynamics of energy deposition in YaJEM is rather different from the Crescendo scenario. The initial branching processes down from a highly virtual state happen very rapidly and lead to a pronounced initial rise in energy deposition as the number of partons undergoing elastic energy loss increases. However, the finite energy of the parton shower that is explicitly considered leads to a turnover: As partons become absorbed by the medium, the number of additionally radiated gluons is limited by kinematic constraints. As a result, the functional shape of $\frac{dE}{dt}$ is decreasing in time, therefore the scenario is henceforth labeled Decreasing.

III. RESULTS

A. Input values and qualitative expectations

In the following results we consider the following situation: A source parton is created at time $t = 0$ and travels through the medium until the energy deposition ceases at time $t = 5$ fm/c. As discussed in Sec. II C, the source parton is assumed to excite the medium through the source term, Eq. (21). We continue to evolve the medium response until time $t = 7$ fm, at which point the medium is assumed to hadronize into the spectrum given by Eq. (12). Performing the freeze-out 2 fm after the source is turned off improves the validity of the linearized hydrodynamic assumption because the peak amplitude of the energy and momentum density perturbations decays in time once the source is turned off.

The underlying medium is at temperature $T_0 = 250$ MeV and has speed of sound $c_s^2 = 1/3$. The shear viscosity-to-entropy density ratio η/s is treated as an input parameter that we vary from $\eta/s = 0.1$–0.2. The range of input values for η/s is consistent with phenomenological observations from heavy-ion collisions [33]. The local excitation parameter λ, mentioned in Sec. II C, is treated as an input parameter, which we vary between 0 and 2 fm. Although we treat λ and η/s as parameters, rigorous determination of their values must come from the underlying theory. One may ask what sets an upper limit for λ. From the point of view of hydrodynamics, λ appears as the coefficient of a gradient, so in principle its value sets a minimum resolution for the hydrodynamic equations of motion. However, in the case we are considering, we allow the medium response to decay in time, improving the validity of hydrodynamics, in particular, linearized hydrodynamics, once the freeze-out occurs. To quantitatively set an upper limit on λ, one must solve for the medium response for a given scenario and see how large the perturbations are. In each of the scenarios we consider here, we find that the linearized approximation holds [to the extent that δu appearing in Eq. (11) remains <1].

The primary goal of this paper is to demonstrate that the time dependence of the energy deposition rate dE/dt, which appears as a coefficient to the source, Eq. (21) is highly relevant for the appearance of a shock-wave signal in the azimuthal spectrum (12). We consider the three energy deposition scenarios, Crescendo, Flat, and Decreasing, discussed in detail in Sec. II D. To make the comparison consistent, in all three scenarios the total energy deposited into the medium is 20 GeV (see Fig. 1). Before examining the results of our calculations it is useful to qualitatively consider what may be expected. From Eqs. (11) and (12) one can see that the appearance of a shock-wave signal is sensitive to the combination $\delta u(x) p_T / T$, where, as discussed in Sec. II B, $\delta u(x)$ is the four-velocity induced by the source. In the limit of validity of linearized hydrodynamics, $\delta u < 1$, thus, as mentioned in a previous work [34], one expects the shock-wave signal to be more pronounced
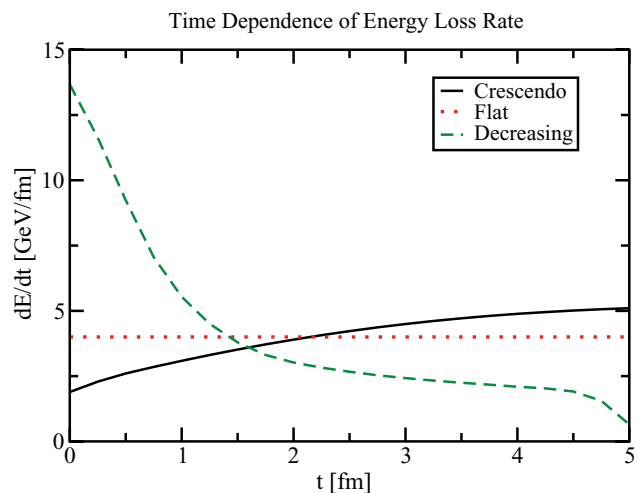

FIG. 1. (Color online) Time dependence of the energy deposition rate into the medium for a given $\Delta E_{tot} = 20$ GeV as calculated in three scenarios—Crescendo, Flat, and Decreasing—for the in-medium evolution of an initial hard parton (see text).

for larger values of p_T/T. However, it is not hard to see that this expectation remains even for nonlinear hydrodynamics. Even if one does not linearize the disturbance created by the hard parton, Eqs. (11) and (12) still predict an enhanced signal for larger p_T.

Experimentally, the opposite trend is seen [8,9]: The double-peaked structure observed in the away-side distribution of dihadron correlations is more pronounced for smaller values of p_T. This observation does not mean that the Mach cone shock wave is not responsible for the double-peaked structure seen experimentally but, rather, exposes the limitations of hydrodynamics. As p_T increases, the driving mechanism behind the correlation structure shifts from bulk recoil to hard fragmentation. Most events produce correlations in the low-p_T hydrodynamical regime, but at higher p_T values, there is an increased bias to see the comparatively rare events in which hard pQCD is the mechanism underlying the correlation. At a p_T beyond 5–6 GeV, these hard events completely dominate the visible correlation. It is this transition from soft to hard physics that governs the transition from shoulder region to head region in the data and is beyond the scope of our current work (see Ref. [35] for an analysis of this transition).

Generally speaking, one would expect that higher amplitudes of the induced energy and momentum density perturbations would be more likely to generate a shock-wave signal in the azimuthal spectrum than lower ones would. In terms of the time dependence of the energy deposition rate dE/dt, the naive expectation is that an energy deposition rate that grows in time is more favorable for the appearance of a shock-wave signal than one that decreases or is flat. To make the argument more concrete, consider a source that deposits some amount of energy and momentum at an instant in time and is then turned off. The time dependence of the medium perturbation owing to such a source can be tracked by going back to Eqs. (3)–(5) and using the reverse Fourier transform (6). Performing the ω integration using contour methods and leaving the **k** integration

undone shows that, to first order in shear viscosity, as a function of time,

$$\delta\epsilon, g_L \sim \exp\left[-\frac{\Gamma_s k^2 t}{2}\right] \tag{39}$$

and

$$g_T \sim \exp\left[-\frac{3\Gamma_s k'^2 t}{4}\right]. \tag{40}$$

The medium excitation decays exponentially as a function of time, meaning that the azimuthal spectrum, Eq. (12), reflects the strength of energy deposition at later times more than that at earlier times. However, the situation is complicated by the fact that the diffusive contribution g_T decays more quickly in time than the sound contribution $\delta\epsilon$ and g_L. It has been mentioned in Sec. II C that the appearance of a shock-wave signal in the azimuthal spectrum will come from $\delta\epsilon$ and g_L, whereas g_T tends to fill up any double-peak structure. Even though the amplitude of the medium excitation decays exponentially in time for both the sound and the diffusion modes, the sound/diffusive ratio contribution actually grows in time. From these considerations, it is not immediately clear whether an energy deposition rate that grows in time or decreases in time is more favorable for generating a shock-wave signal. In Sec. III B we present the results of our calculations.

B. Numerical results

In this section we present results for the azimuthal hadron spectrum, Eq. (12), obtained using the medium parameters and energy deposition scenarios discussed. In all results we show the spectrum for the three energy deposition scenarios, Crescendo, Flat, and Decreasing, and for the bins $p_T = 2$–3 and $p_T = 3$–4 GeV. Results for a shear viscosity-to-entropy density ratio $\eta/s = 0.10$ and local excitation parameter $\lambda = 0$ fm (λ is discussed in Sec. II C) are shown in Fig. 2.
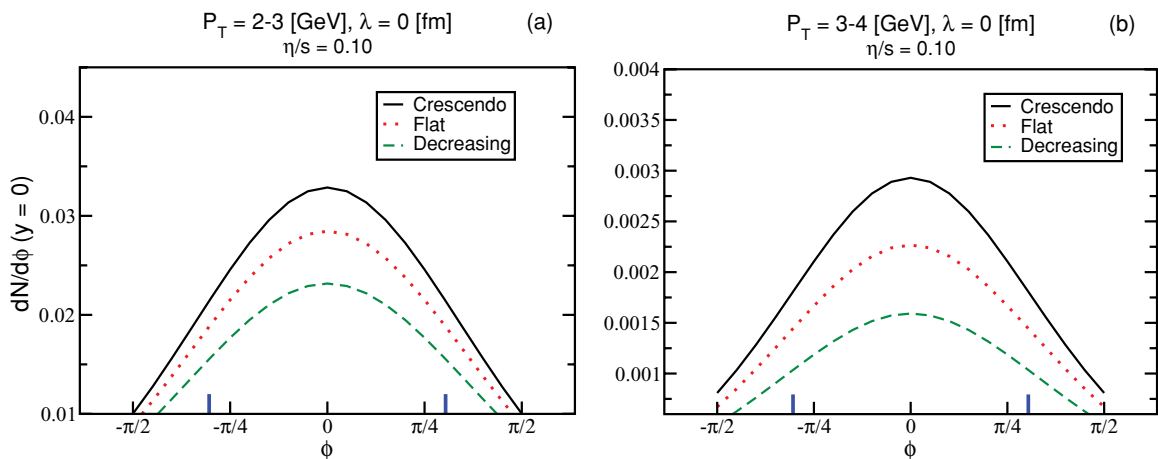

FIG. 2. (Color online) Azimuthal hadron spectrum, Eq. (12), for the case of $\eta/s = 0.10$ and local excitation parameter, $\lambda = 0$ fm. The shapes of the spectra for the different energy deposition scenarios are essentially the same for these parameters. The magnitude of the signal is larger for Crescendo, which grows in time, than for Flat or Decreasing, even though the same total energy is deposited in each case. The conical structure generated by the source, Eq. (21), when $\lambda = 0$ fm is not strong enough to overcome the diffusive wake in the final spectra, where one sees a single peak at $\phi = 0$, which defines the direction of source propagation. The larger (blue) tick marks on the ϕ axis indicate where one would naively expect conical peaks to appear for the speed of sound used here, $\phi = \arccos c_s$.
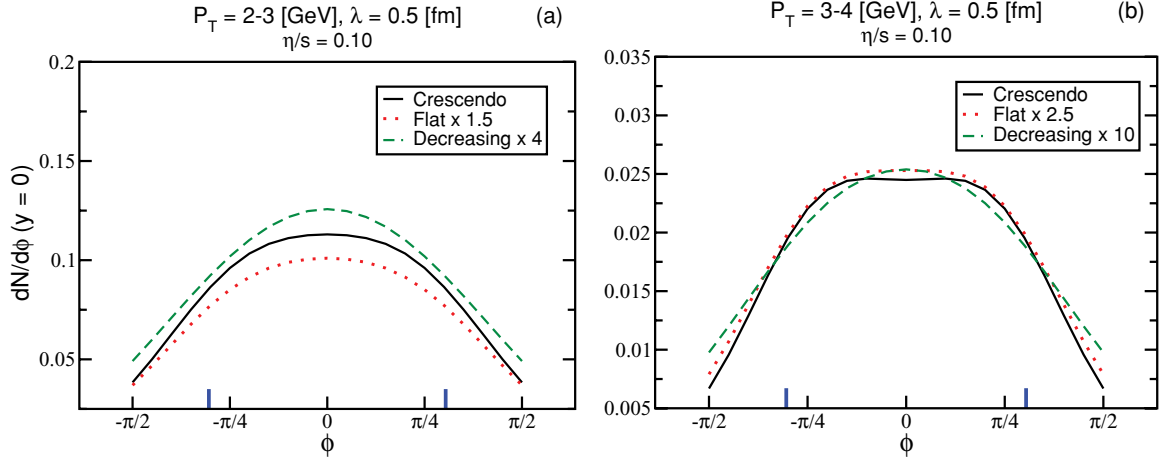
FIG. 3. (Color online) The same as Fig. 2, but for $\lambda = 0.5$ fm. The spectrum is noticeably flatter than that seen in the $\lambda = 0$ fm case, especially for the $p_T = 3 - 4$ GeV plot, where a double-peak begins to emerge in the Crescendo curve. The difference in the shapes of the spectra generated by the different energy deposition scenarios is most noticeable in comparing the Crescendo and Decreasing scenarios. The energy deposition that grows in time generates a stronger conical signal. The larger (blue) tick marks on the ϕ axis indicate where one would naively expect conical peaks to appear for the speed of sound we have used.

Recall that the direction of the source propagation determines the direction of $\phi = 0$ in our plots. The results show that the shape of the spectrum is roughly the same for all three energy deposition scenarios, however, the magnitude of the signal is larger for Crescendo, which grows in time, than for Flat or Decreasing. This change in magnitude between the different energy deposition scenarios reflects the viscous nature of the medium. Energy that is deposited at earlier times (such as in the Decreasing scenario) has more time to equilibrate with the background medium before freeze-out. What is noticeably missing in Fig. 2 is the appearance of a double-peaked structure, or shock-wave signal. Apparently the conical structure generated by the source, Eq. (21), when $\lambda = 0$ fm is not strong enough to overcome the diffusive wake in the final spectrum.

Next we consider results for $\eta/s = 0.10$ and $\lambda = 0.5$ fm, which are shown in Fig. 3. The spectrum is noticeably flatter than seen in the $\lambda = 0$ fm case, especially for the $p_T = 3$– 4 GeV plot, where a double-peak begins to emerge in the Crescendo curve. Note that not only the magnitudes of the curves for the different energy deposition scenarios, but also the shapes, are different. The difference is most noticeable in comparing the Crescendo and Decreasing scenarios. The shape of the Decreasing spectrum is very similar to the case of $\lambda = 0$ fm, however, the shape of the Crescendo spectrum is much flatter, even showing a slight dip at $\phi = 0$. The energy deposition that grows in time appears to generate a cleaner signal of the underlying conical structure induced in the medium.

We continue by considering results for $\eta/s = 0.10$ and $\lambda = 1.0$ fm presented in Fig. 4. Here the double-peaked
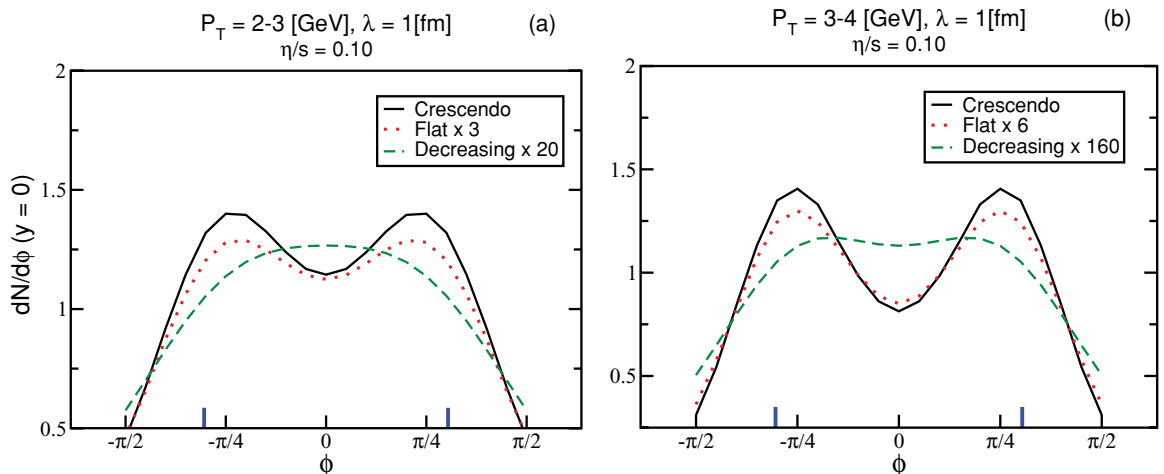
FIG. 4. (Color online) The same as Figs. 2 and 3, but for $\lambda = 1.0$ fm. The double-peaked structure is significantly enhanced, particularly in the Crescendo and Flat spectra. The difference in the shapes of the spectra generated by the different energy deposition scenarios is obvious. The larger (blue) tick marks on the ϕ axis indicate where one would naively expect conical peaks to appear for the speed of sound used here.
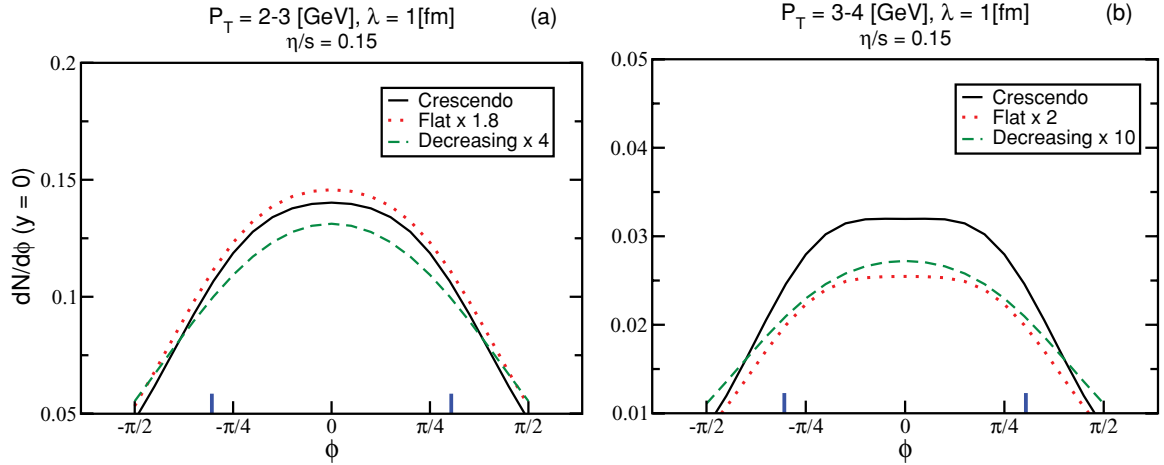
FIG. 5. (Color online) The azimuthal hadron spectrum, Eq. (12), for the case of $\eta/s = 0.15$ and $\lambda = 1.0$ fm. The effect of viscosity to smear out any double-peaked structure is obvious upon comparison to the results in Fig. 4, where we consider $\eta/s = 0.10$ and $\lambda = 1.0$ fm. The larger (blue) tick marks on the ϕ axis indicate where one would naively expect conical peaks to appear for the speed of sound used here.

structure becomes quite pronounced for the Flat and Crescendo curves, however, the Decreasing result remains mostly flat, with a slight dip at $\phi = 0$ in the $p_T = 3$–4 GeV range. The Flat and Crescendo spectra have a similar shape, however, the Crescendo result shows a moderately more pronounced double-peak. The trend is emerging that for fixed values of η/s and increasing values of λ, an energy deposition scenario that increases in time generates a more pronounced shock-wave signal in the final azimuthal spectrum.

The results for $\eta/s = 0.15$ and $\lambda = 1.0$ fm are shown in Fig. 5. By comparison with Fig. 4, one can see that a 50% increase in the shear viscosity has a significant effect on the final azimuthal spectrum. The double-peaked shock-wave signature has been smeared out by the viscous effects. Continuing with $\eta/s = 0.15$ and increasing λ to 1.5 fm restores the shock-wave signal in the Flat and Crescendo energy deposition scenarios, as is evident from Fig. 6. However,

consistent with the preceding results, the Decreasing energy deposition remains mostly flat. Finally, we present results for $\eta/s = 0.20$ and $\lambda = 2.0$ fm in Fig. 7. Again, the result of increasing the viscosity is to smear out the double-peaked structure, even though we have increased λ by the same fraction.

Here we discuss the form of the source, Eq. (24), which we have employed for the results already presented. As mentioned briefly in Sec. II C, we do not include a time derivative on dE/dt or boundary terms that arise from the source being turned on and off at $t = 0$ and $t = T$. As noted, we have explicitly checked that the derivative term is numerically insignificant for the energy deposition scenarios we consider and can safely be ignored. However, the boundary terms—in particular, the term resulting from turning the source off at time $t = T$—is not numerically insignificant. In fact, the effect of the boundary term at $t = T$ is to create a strong inward flow
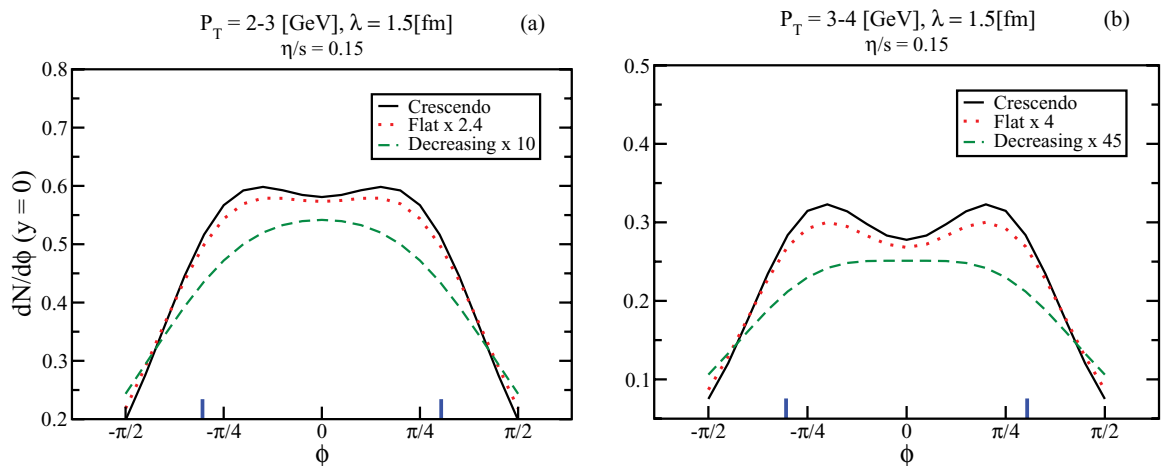

FIG. 6. (Color online) Azimuthal hadron spectrum for $\eta/s = 0.15$ and $\lambda = 1.5$ fm. Increasing λ restores the shock-wave signal in the Flat and Crescendo energy deposition scenarios (compare to Fig. 5, where $\lambda = 1.0$). However, consistent with these results, the Decreasing energy deposition remains mostly flat. The larger (blue) tick marks on the ϕ axis indicate where one would naively expect conical peaks to appear for the speed of sound used here.
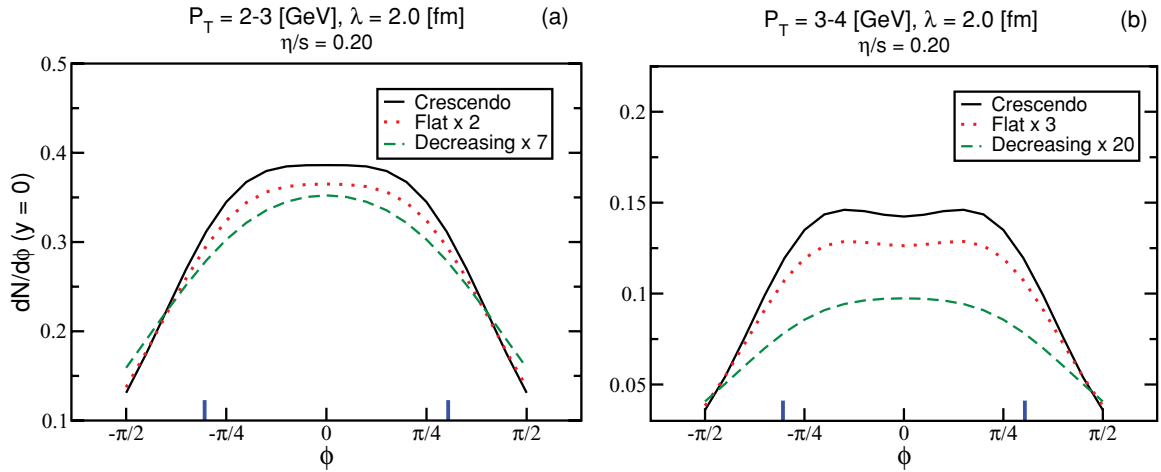
FIG. 7. (Color online) Resulting spectra for $\eta/s = 0.20$ and $\lambda = 2.0$ fm. Again, the result of increasing the viscosity is to smear out the double-peaked structure, even though we have increased λ by the same fraction as presented in Fig. 6. Recall that the larger (blue) tick marks on the ϕ axis indicate where one would naively expect conical peaks to appear for the speed of sound used here.

as the source is absorbed by the medium. This inward flow tends to destroy the conical Mach cone signal and reduce the differences in the three scenarios.

This feature is demonstrated in Fig. 8, where we show the azimuthal spectrum for the bin $p_T = 2$–3 GeV, $\eta/s = 0.10$, and $\lambda = 1.25$ fm. The left plot in Fig. 8 shows the result without including the boundary and derivative terms, whereas the right plot contains those contributions (they are dominated by the $t = T$ boundary piece). The left plot is characteristic of the plots already shown, in that the Crescendo curve has the most pronounced double-peak structure, whereas the Flat and Decreasing curves are less pronounced. In the right plot in Fig. 8, however, one sees that the difference in the shapes of the curves is less significant and, also, narrower. This results

directly from inward flow created by the absorption of the source at an instant in time.

The absorption at $t = T$ is an artifact of our procedure to stop the simulation and tends to obscure the physics we are trying to study. In a real physical situation, the source is not simply absorbed at some fixed instant but may escape the medium, run out of energy, etc. With an infinite-energy (for the case of the Crescendo and Flat scenarios), static-medium assumption, the problem of stopping the energy deposition is not well defined (it would go on forever), so we have to make a choice as to what we want to show as a freeze-out distribution. We believe that we can get closer to what we are interested in by dropping the boundary terms—which we have done in the preceding. However, the complications just described illustrate
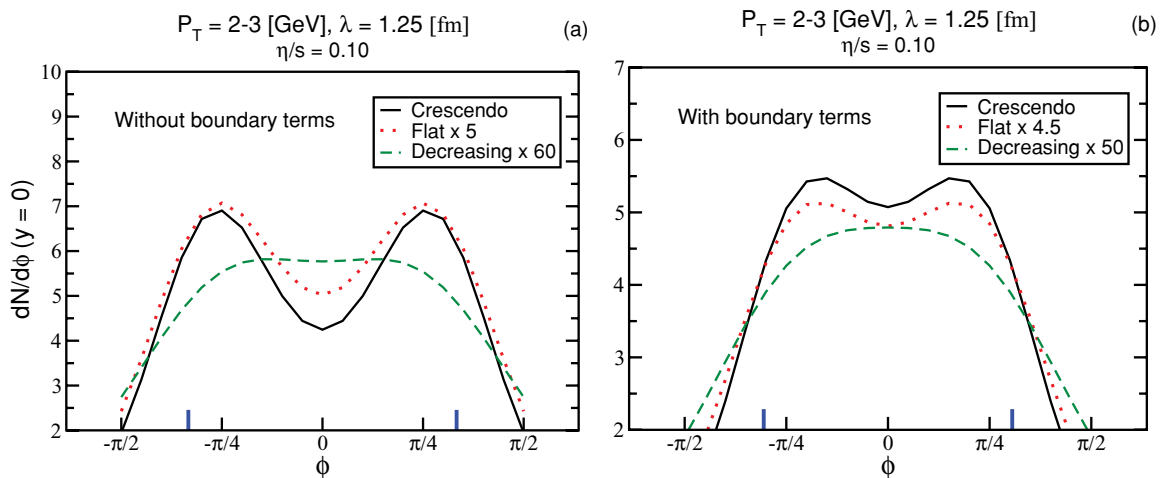

FIG. 8. (Color online) Results for $p_T = 2$–3 GeV, $\eta/s = 0.10$, and $\lambda = 1.25$ fm. The left plot shows the result without including the boundary and derivative terms (as discussed in the text), whereas the right plot contains those contributions. In the right plot, one sees that the differences in the shapes of the curves are less significant and, also, narrower. This results from inward flow created by the absorption of the source at an instant in time and is an artifact of an infinite-energy (for the case of the Crescendo and Flat scenarios), static-medium assumption. We have not included the boundary terms in these results, as they obscure the physics we are trying to study. The larger (blue) tick marks on the ϕ axis indicate where one would naively expect conical peaks to appear for the speed of sound used here.

the need for a more realistic description of both the medium evolution and the source term.

We conclude this section by briefly considering how our results depend on the specific choice of speed of sound $c_s^2 = 1/3$ and temperature $T_0 = 250$ MeV that we have used here. Both the speed of sound and the temperature appear explicitly in the medium distribution function [see Eqs. (8) and (11)] used for freeze-out. Changing the temperature in the medium distribution function, Eq. (11), will have an effect on the strength of the freeze-out signal. Specifically, lowering the temperature will tend to generate a stronger signal. Likewise, lowering the speed of sound in the medium distribution function will also tend to create a stronger freeze-out signal (even more so than the temperature, as the speed of sound appears only with the momentum flow).

The temperature also enters the sound attenuation length, $\Gamma_s = \frac{4\eta}{3sT}$, which appears in the equations of motion for linearized hydrodynamics, Eqs. (3)–(5). Changing the temperature in Γ_s is effectively like changing η/s, which has been analyzed in the preceding results, thus we do not consider that aspect further here. However, the speed of sound appears in a nontrivial way in the equations of motion. As is well understood, the speed of sound governs the angle of propagation of Mach cone shock waves generated by a projectile. We present in Fig. 9 the effects of changing the speed of sound on the azimuthal hadron spectrum for the Crescendo and Flat energy deposition scenarios and for the bin $p_T = 2$–3 GeV. The results are for $\eta/s = 0.10$, $\lambda = 1$ fm, and speed of sound $c_s = 0.577$ and $c_s = 0.5$. As anticipated, the spectrum becomes more pronounced when
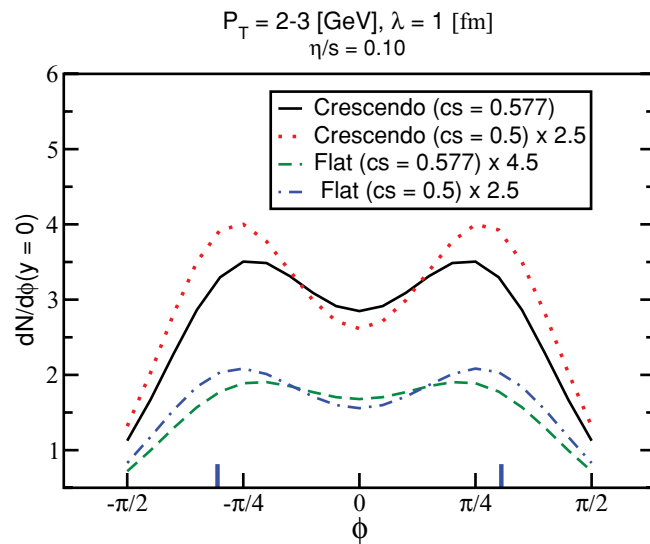

$P_T = 2$-3 [GeV], $\lambda = 1$ [fm]
$\eta/s = 0.10$

Legend:
— Crescendo (cs = 0.577)
···· Crescendo (cs = 0.5) x 2.5
–·– Flat (cs = 0.577) x 4.5
–·– Flat (cs = 0.5) x 2.5

FIG. 9. (Color online) Results for $p_T = 2$–3 GeV, $\eta/s = 0.10$, and $\lambda = 1.0$ fm with two different speeds of sound. As discussed in the text, one would anticipate that the spectrum will become more pronounced upon lowering the speed of sound and that the peaks will appear at larger opening angles. These two features are indeed observed. However, note that the peak angles do not correspond to a naive prediction based on purely geometric arguments [the larger (blue) ticks on the ϕ axis would naively correspond to $c_s = 0.577$] even for the simple scenario considered here.

lowering the speed of sound, and the peaks also appear at larger opening angles. However, note that the peak angles do not correspond to a naive prediction based on purely geometric arguments even for the simple scenario considered here [the larger (blue) ticks on the ϕ axis in Fig. 9 would naively correspond to $c_s = 0.577$]. One thus needs to be very careful not to interpret the experimentally measured opening angle of the correlation geometrically as being directly related to the speed of sound: In a realistic medium, the combination of trigger bias with a longitudinal, transverse, and elliptic flow field will have an even more significant influence on the angular structure than in our simplified medium study.

IV. CONCLUSIONS

We have conducted a systematic study of shock-wave excitation for different models of the spatiotemporal structure of energy deposition into the medium within a linearized hydrodynamical framework in a constant medium under different assumptions with regard to medium properties and the interaction of the source with the medium. The results exhibit a few generic trends, as follows.

(i) Only a strong gradient term ($\lambda > 0$) in the source, Eq. (21), leads to an observable double-hump structure. The observation that a gradient term is necessary to excite an observable double-peak was made early on [10], however, our implementation of the source, Eq. (21), provides a way to quantify how strong the gradient term must be.

(ii) For a fixed strength of the gradient term, viscous effects (i.e., larger values of η/s) weaken the double-hump structure. This has a natural explanation in terms of entropy generation dissipating the shock wave, but even for relatively small η/s the effect appears rather pronounced.

(iii) Consistently for all assumptions about the structure of the source term and the medium shear viscosity, an energy deposition dE/dt that increases as a function of time leads to more pronounced shock-wave-like correlations than a dE/dt that decreases in time—both in the absolute strength of the correlation and in the shape. This effect is not small—the correlation strength can be reduced more than an order of magnitude in the Decreasing compared to the Crescendo scenario— although the precise factor depends on the medium properties.

Applied to the shock-wave interpretation of measured correlations in heavy-ion collisions, these findings imply that the measured signal depends strongly on the medium properties, the local structure of the source term, and the spatiotemporal pattern of energy deposition. Thus, if one is able to model the evolution of an initial hard parton and its interaction with the medium with sufficient precision, one can determine medium parameters like η/s from the measured correlations. In contrast, if one can extract the medium properties with other methods, the correlations then place tight constraints on the dynamics of hard parton evolution in the medium. Which road will be taken first remains to be seen.

[1] M. Gyulassy and X. N. Wang, Nucl. Phys. B **420**, 583 (1994).

[2] R. Baier, Y. L. Dokshitzer, A. H. Mueller, S. Peigne, and D. Schiff, Nucl. Phys. B **484**, 265 (1997).

[3] B. G. Zakharov, JETP Lett. **65**, 615 (1997).

[4] U. A. Wiedemann, Nucl. Phys. B **588**, 303 (2000).

[5] M. Gyulassy, P. Levai, and I. Vitev, Nucl. Phys. B **594**, 371 (2001).

[6] X. N. Wang and X. F. Guo, Nucl. Phys. A **696**, 788 (2001).

[7] M. Shimomura (PHENIX Collaboration), arXiv:nucl-ex/0510023.

[8] S. S. Adler *et al.* (PHENIX Collaboration), Phys. Rev. Lett. **97**, 052301 (2006).

[9] J. Adams *et al.* (STAR Collaboration), Phys. Rev. Lett. **95**, 152301 (2005); J. G. Ulery (STAR Collaboration), Nucl. Phys. A **774**, 581 (2006).

[10] J. Casalderrey-Solana, E. V. Shuryak, and D. Teaney, J. Phys. Conf. Ser. **27**, 22 (2005)

[11] T. Renk and J. Ruppert, Phys. Rev. C **73**, 011901 (2006).

[12] T. Renk and J. Ruppert, Phys. Lett. B **646**, 19 (2007).

[13] T. Renk and J. Ruppert, Phys. Rev. C **76**, 014908 (2007).

[14] R. B. Neufeld, B. Müller, and J. Ruppert, Phys. Rev. C **78**, 041901 (2008); B. Muller and R. B. Neufeld, J. Phys. G **35**, 104108 (2008).

[15] R. B. Neufeld, Phys. Rev. D **78**, 085015 (2008).

[16] R. B. Neufeld, Phys. Rev. C **79**, 054909 (2009).

[17] B. Betz, M. Gyulassy, J. Noronha, and G. Torrieri, Phys. Lett. B **675**, 340 (2009).

[18] J. Noronha and M. Gyulassy, arXiv:0806.4374 [hep-ph].

[19] R. B. Neufeld and B. Muller, Nucl. Phys. A **830**, 789C (2009); Phys. Rev. Lett. **103**, 042301 (2009).

[20] G. Y. Qin, A. Majumder, H. Song, and U. Heinz, Phys. Rev. Lett. **103**, 152303 (2009).

[21] I. G. Bearden *et al.* (BRAHMS Collaboration), Phys. Rev. Lett. **90**, 102301 (2003).

[22] U. W. Heinz, arXiv:0901.4355 [nucl-th].

[23] F. Cooper and G. Frye, Phys. Rev. D **10**, 186 (1974).

[24] B. Betz, J. Noronha, G. Torrieri, M. Gyulassy, I. Mishustin, and D. H. Rischke, Phys. Rev. C **79**, 034902 (2009).

[25] P. M. Chesler and L. G. Yaffe, Phys. Rev. D **78**, 045013 (2008).

[26] M. H. Thoma, Phys. Lett. B **273**, 128 (1991).

[27] C. A. Salgado and U. A. Wiedemann, Phys. Rev. D **68**, 014008 (2003).

[28] T. Renk, Phys. Rev. C **78**, 034908 (2008).

[29] T. Renk, Phys. Rev. C **79**, 054906 (2009).

[30] V. N. Gribov and L. N. Lipatov, Sov. J. Nucl. Phys. **15**, 438 (1972); Yu. L. Dokshitzer, Sov. J. Phys. JETP **46**, 641 (1977).

[31] G. Altarelli and G. Parisi, Nucl. Phys. B **126**, 298 (1977).

[32] M. Bengtsson and T. Sjöstrand, Phys. Lett. B **185**, 435 (1987); Nucl. Phys. B **289**, 810 (1987); E. Norrbin and T. Sjöstrand, *ibid.* **603**, 297 (2001).

[33] P. Romatschke and U. Romatschke, Phys. Rev. Lett. **99**, 172301 (2007).

[34] J. Casalderrey-Solana, E. V. Shuryak, and D. Teaney, arXiv:hep-ph/0602183.

[35] T. Renk, Phys. Rev. C **78**, 014903 (2008).